Best Student Paper Award

Performance and Modeling of Active Metal-Matrix Composites Manufactured by Ultrasonic Additive Manufacturing

Ryan Hahnlen, Marcelo J. Dapino

Smart Vehicle Concepts Center, The Ohio State University, Columbus, OH, USA, 43210

ABSTRACT

This paper presents the development and characterization of active aluminum-matrix composites manufactured by Ultrasonic Additive Manufacturing (UAM), an emerging rapid prototyping process based on ultrasonic metal welding. The primary benefit of UAM over other metal-matrix fabrication processes is the low process temperatures, as low as 25 °C. UAM thus provides unprecedented opportunities to develop adaptive structures with seamlessly embedded smart materials and electronic components without degrading the properties that make these materials and components attractive. The objective of this research is to develop UAM composites with aluminum matrices and embedded shape memory NiTi, magnetostrictive Galfenol (FeGa), and polyvinylidene fluoride (PVDF) phases. The paper is focused on the thermally induced strain response and stiffness behavior of NiTi-Al composites, the actuation properties of FeGa-Al composites, and the embedded sensing capabilities of PVDF-Al composites. We observe up to a 10% increase over room temperature stiffness for NiTi-Al composites and a magnetomechanical response in the FeGa-Al composite up to 52.4 $\mu\epsilon$. The response of the PVDF-Al composite to harmonic loads is observed over a frequency range of 10 to 1000 Hz.

Keywords: NiTi, Galfenol, magnetostriction, PVDF, metal-matrix composite, active composites, ultrasonic additive manufacturing, ultrasonic consolidation

1. INTRODUCTION

Metal-matrix composites enable seemingly homogeneous structures to have augmented mechanical properties that surpass those of the parent materials. Smart composites enable structures with embedded multifunctionality. Embedding smart materials within a metal matrix can be challenging as methods for metal-matrix composite construction typically require temperatures near or above the melting point of the matrix material. Even in processes that do not require melting, such as powder metallurgy utilizing diffusion bonding, temperatures can reach over 560 °C.[1] Processes with high temperatures and stresses are generally not conducive to smart material design as this can reduce or eliminate the unique properties that make these materials useful. In contrast to typical metal-matrix composite construction methods, Ultrasonic Additive Manufacturing (UAM) is a rapid prototyping process that can create metal matrix composites at room temperature. UAM is used in this study to create composites consisting of an aluminum (Al) matrix and seamlessly embedded smart materials.

UAM incorporates the principles of ultrasonic metal welding and subtractive processes to create metal parts with arbitrary shapes and embedded materials.[2] UAM offers unprecedented opportunities to create parts with embedded smart materials (e.g., shape memory alloys, fiber optics, or electroactive polymers) and electronic components. The key features of UAM are shown in Fig. 1. Vibrations generated by a piezoelectric ultrasonic transducer are transmitted into the parts through a rolling sonotrode. The vibrations propagate longitudinally from the transducer to the sonotrode through tuned waveguides while normal force is applied to the vibrating sonotrode as it rolls along the work piece. The vibrations are transmitted to the weld interface causing relative motion between the top tape layer and the surface below. This relative interface motion causes shear deformations of contacting surface asperities, dispersing interface oxides, and ultimately bringing clean metal-to-metal contact and metallic bonding between the work pieces.[3] The current UAM systems achieve the most effective bonding

Further author information: (Send correspondence to M.J.D)
R.H.: E-mail: hahnlen.1@osu.edu, Telephone: 1-614-247-7480
M.J.D.: E-mail: dapino.1@osu.edu, Telephone: 1-614-688-3689

Industrial and Commercial Applications of Smart Structures Technologies 2011,
Edited by Kevin M. Farinholt, Steve F. Griffin, Proc. of SPIE Vol. 7979, 797903
 · doi: 10.1117/12.881152

on thin metal layers 0.152 mm (0.006 in) thick. The UAM system therefore creates larger bulk builds by welding successive layers of metal tapes or sheets.

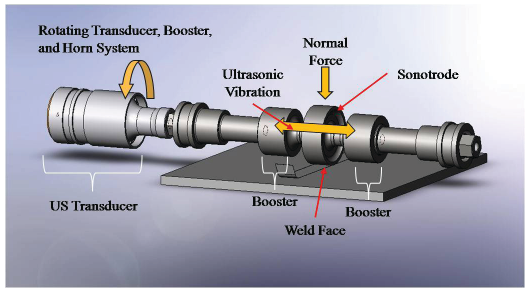

Figure 1. In the UAM process, successive layers of metal tape are bonded together for creating metallic composites with seamlessly embedded materials and features.

The smart materials studied in this research are NiTi, Galfenol (FeGa), and polyvinylidene fluoride (PVDF). The unique properties of NiTi are a result of stress and temperature induced transformations between martensite and austenite. Under no stress, martensite forms in the twinned or self-accommodating phase. With the application of stress at low temperature, martensite detwins resulting in a large recoverable detwinning strain. Upon heating, the martensite transforms to austenite ($M - A$) which recovers the induced detwinning strain. With the application of a temperature dependent stress, the austenite can also transform to detwinned martensite ($A - M$) which also induces large strains. If stress is released and temperature remains constant, the $M - A$ transformation occurs and induced detwinning strain is again recovered. The $M - A$ transformation is accompanied by an increase in elastic modulus of over 100%,[4] an induced strain recovery of up to 8%,[5] and a large change in electrical resistivity.[6,7]

Galfenol (FeGa) is a magnetostrictive material that produces a strain in response to applied magnetic fields or, inversely, becomes magnetized in response to applied stresses. For this research, an FeGa-Al composite was constructed and its actuation properties studied in order to understand and determine the coupling between the active FeGa phase and passive Al matrix. Ensuring that there is maximum mechanical coupling between the FeGa phase and Al matrix is of critical importance for both sensing and actuation.

Electroactive PVDF is a piezoelectric material which produces a charge in response to applied stresses. The embedding process ensures the PVDF polymer is protected from harsh environmental conditions and less susceptible to mechanical damage. In this research we quantify the frequency response of a PVDF-Al composite and compare it to a reference sample of PVDF.

2. NICKEL TITANIUM-ALUMINUM UAM COMPOSITES

2.1 NiTi-Al composite methods

2.1.1 Composite construction

Three NiTi-Al composites were constructed through UAM. All composites were made by embedding 0.254 mm by 0.762 mm (0.01 in by 0.03 in) NiTi ribbons at the midpoint of an Al 3003-H18 matrix made with four 0.152 mm (0.006 in) thick tapes. Prior to embedding, the NiTi ribbons were heated and allowed to cool to ensure that they were in a fully twined martensitic state. After twinning the martensite, the NiTi ribbons were placed in an embedding fixture. The NiTi ribbon used in these composites was studied to determine its transition temperatures though thermal cycling and resistance measurements. The transition temperatures are 52°C and 56°C for A_s and A_f, and 42°C and 48°C for M_f and M_s, respectively.

Each composite has a different volume fraction of NiTi as controlled by the number of ribbons embedded and the total cross sectional dimensions of the composites. Composite 1 has a single embedded ribbon and was machined to have a 5% NiTi volume fraction. Composites 2 and 3 have two NiTi ribbons and were machined to final dimensions as to have 15% and 20% NiTi volume fractions, respectively. Dimensions and embedded ribbon information is shown in Table 1.

Table 1. Dimensions and NiTi content of NiTi-Al composites.

Composite	Number of Ribbons	Cross Sectional Area [mm^2]	NiTi Volume Fraction
1	1	3.52	5%
2	2	2.54	15%
3	2	1.88	20%

2.1.2 Thermally induced strain

Each of the three NiTi-Al composites and a reference sample of Al 3003 were placed in a thermal chamber and cycled three times from 25 °C to 100 °C and allowed to cool. During thermal cycles, the strain of each composite was measured with a strain gage matched to aluminum alloys and the temperature of the composites was monitored with a thermocouple placed next to the strain gages.

Since the Coefficient of Thermal Expansion (CTE) of the reference sample is known, the strain signal from the Al 3003 sample was used to remove the thermal output of the strain gages from the composite strain signals. To determine the composite strain, the strain measured from the reference sample was subtracted from the strain measured from each composite and then the calculated thermal strain of the reference sample was added to the composite strain measurements:[8]

$$\epsilon_{comp} = \epsilon_{sig/comp} - \epsilon_{sig/ref} + \alpha_{ref} \times \Delta T. \tag{1}$$

Here, $\epsilon_{sig/comp}$ is the non-compensated strain signal from the composite, $\epsilon_{sig/ref}$ is the strain signal from the reference sample, α_{ref} is the CTE of the reference material[9] (23.2 ppm/°C), and ΔT is the change in temperature.

2.1.3 Static axial stiffness tests

The mechanical stiffness of each composite and a reference piece of Al 3003 was measured at three different nominal temperatures, 25 °C, 55 °C, and 100 °C using a tension/compression load frame. At each temperature the composites were first given a nominal tensile reference load of 22.2 N (5 lbf), then load was increased to a nominal tensile load of 66.7 N (15 lbf) under displacement control at a rate of 2.54 mm/s (0.1 in/sec). During loading, the composite's strain was measured using strain gages. Stiffness was then calculated by dividing the change in load between the reference and maximum loads by the change in displacement measured from the strain gage at these load levels. This procedure assumes that the composites exhibit a linear stress/strain behavior which holds as long as the embedded NiTi ribbons are not stressed above the detwinning stress during room temperature loading or do not undergo a stress-induced $A - M$ transformation during loading at elevated temperatures. The possibility of transformation is discussed in section 2.2.2.

2.1.4 Axial natural frequency tests

NiTi-Al composites and an Al 3003 reference sample were also tested to determine their axial natural frequency. In this test, the composites were attached to an inverted shaker and fitted with an end mass with a 3-axis accelerometer at the free end. The end mass and accelerometer have a total mass of 20.98 grams (0.741 oz). The shaker was excited with a stepped sine waveform with excitation frequencies ranging from 50 Hz to 5000 Hz. The 3-axis accelerometer was used to monitor motion in bending and axial directions of the composite. This was done to ensure that bending modes, that could affect axial measurements, were not excited. The mounting plate of the shaker also had an accelerometer which was used to measure the excitation of the composite-end mass system. The stepped sine tests were run at 25 °C and 100 °C. The peak in magnitude of the acceleration ratio transfer function, a_{end}/a_{ref}, was used to determine the natural frequency of each test, where a_{end} is the acceleration of the end mass in the axial direction and a_{ref} is the input acceleration as measured from the shaker accelerometer.

2.2 NiTi-Al composite experimental results and discussion

2.2.1 Thermally induced strain

The temperature versus strain plots of each composites are shown in Fig. 2 (a)-(c). For each composite, the initial cycle is different than subsequent cycles, which stabilize for all composites. This is due to residual detwinning

from loading the composites similar to an effect seen in thermal cycling of constrained shape memory alloys.[10] For clarity, cycles 2 and 3 for each composite are shown in Fig. 2 (d)-(f) without the initial thermal cycles.

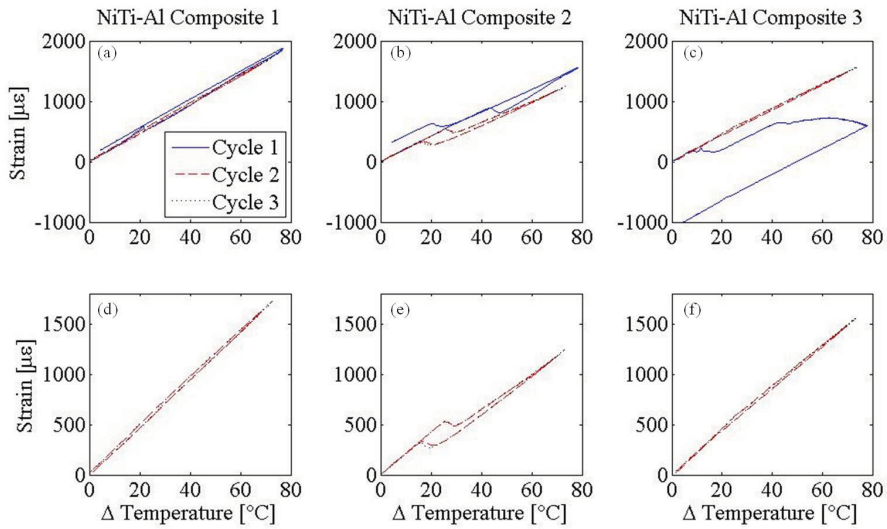

Figure 2. Temperature versus strain plots for cycles 1 through 3 of NiTi-Al: (a) composite 1; (b) composite 2; (c) composite 3. Cycles 2 and 3 only of NiTi-Al: (d) composite 1; (e) composite 2; (f) composite 3.

Composite 1 has a strain spike in the initial cycle after which its behavior becomes strongly linear. The spike in the initial cycle, seen at a ΔT of 20°C, may be due to a stick-slip condition that developed between the ribbon and matrix, allowing the embedded ribbon to contract slightly within the matrix. If this occurred, the matrix would have a momentary increase in strain before being constrained again by the NiTi ribbon, which coincides with what is observed.

The temperature-strain diagram for the second and third thermal cycles of composite 1, Fig. 2 (d), shows a nearly linear behavior. Upon close inspection, the curve has two separate linear regions with a transition occurring approximately between 40°C and 60°C (corresponding to ΔT between 15°C and 25°C). The slopes are found to be 23.6 and 23.5 $\mu\epsilon/°$C for the low temperature slope and high temperature slope, respectively. The relationship between the slopes corresponds to transformation of the embedded NiTi. For a long fiber reinforced composite, the CTE along the fiber direction is a function of the CTEs of the matrix and fiber as well as the elastic moduli of each component,[11,12]

$$\alpha_{comp} = \frac{(1-f)(E_{Al})(\alpha_{Al}) + f(E_{NiTi})(\alpha_{NiTi})}{(1-f)(E_{Al}) + f(E_{NiTi})}, \tag{2}$$

where E_{Al}, E_{NiTi}, α_{Al}, α_{NiTi}, are the elastic moduli and CTEs for Al 3003-H18 and NiTi, respectively, and f is the NiTi volume fraction of the composite. While the NiTi CTE does not change, the change in modulus occurring in the $M-A$ transformation will cause a change in the composite CTE. In this case, the amount of NiTi is relatively small, 5%. As such, the change in CTE is also small and not largely different from that of the Al.

The temperature-strain behavior of composite 2 is significantly different than that of composite 1. After an initial linear region, the composite recovers some strain as observed by a contraction seen in Fig 2 (b) and (e). After a repeatable amount of contraction, the composite again behaves linearly with a different CTE than the initial low temperature region. Upon cooling, the process reverses with the exception of a hysteretic recovery of the thermal contraction. The strain recovery suggests that there is some amount of prestrain in the embedded NiTi. Upon heating through A_s and A_f, the $M-A$ transformation recovers the prestrain and generates recovery stresses, causing the observed contraction. Upon cooling, the $A-M$ transition occurs over M_s and M_f which produce the observed hysteresis.

Composite 3 has linear behavior similar to composite 1 in its second and third cycles. However since composite 3 has high a higher NiTi volume fraction than composite 2, we would expect a similar response and larger magnitude of strain recovery. An explanation for the behavior of composite 3 is in the strain response from the initial thermal cycle. In the first cycle, Fig. 2 (c), composite 3 exhibits an initial linear region followed by a strain recovery greater in magnitude than composite 2. After this recovery there is a gradual decrease in slope which becomes negative before cooling begins. This gradual slope change and strain recovery is hypothesized to be plastic deformation of the Al matrix from the generation of recovery stresses in the NiTi.

As a prestrained NiTi sample is heated under constraint, it generates a recovery stress that increases with temperature. In being heated to 100°C, the NiTi ribbons in composite 3 appear to generate enough recovery stress to yield the matrix, allowing the ribbons to recover any induced prestrain. This scenario requires that the NiTi ribbons have an initial prestrain, similar to the hysteretic behavior of composite 2. In subsequent thermal cycles, composite 3 had no remaining prestrain and therefore behaved in a piecewise linear fashion similar to composite 1 with two linear regions.

The behavior of these composites suggests that although steps were taken to embed the NiTi ribbons without prestrain, manufacturing of the composites did induce strain in the NiTi ribbons during embedding. The rolling action of the UAM horn and plastic embedding of the ribbons into the matrix likely induced detwinning of the martensitic structure of the NiTi thus creating a prestrain. All three composites, having been constructed via UAM, likely had an amount of prestrain induced. For composites 1 and 3, the initial heating cycles appear to have removed the initial prestrain through movement of the embedded ribbon in composite 1 or through deformation of the matrix in composite 3. In creating and modeling shape memory alloy composites, prestrain is an important factor that has significant influence on their thermomechanical behavior.[13,14] As such, ongoing work is focused on the analytical modeling of these composites considering the effects of prestrain and matrix constraint.

The thermally induced strain for NiTi-Al composite 2 is the subject of an empirical model. Composites 1 and 3 follow a similar procedure but have a difference in calculating the recovery strain which is noted. First, from the thermally induced strain data, the composite CTEs associated with the martensitic and austenitic phases of the embedded NiTi, α_m and α_a respectively, were measured by finding the slopes of the linear regions shown in Fig 2 (e).

Next, the composite CTE was calculated using a temperature induced transformation based upon the Brinson model for 1-D shape memory alloys.[15] In this model, the CTE is equal to α_m when temperatures are below A_s when heating and below M_f during cooling. Similarly, the composite CTE is equal to α_a when temperatures surpass A_f during heating and remain above M_s during cooling. In the transition regions the composite CTE is calculated by

$$\alpha_{comp}(T) = \zeta\alpha_m + (1-\zeta)\,\alpha_a \tag{3}$$

where

$$\zeta = 1/2 + 1/2cos\left[\pi\frac{(T-A_s)}{(A_f-A_s)}\right] \tag{4}$$

when $A_s \leq T \leq A_f$ during heating and

$$\zeta = 1/2 + 1/2cos\left[\pi\frac{(M_s-T)}{(M_s-M_f)}\right] \tag{5}$$

when $M_f \leq T \leq M_s$ during cooling. The transition temperatures used were found through previous experiments in which the electrical resistance of the NiTi wire was observed as a function of temperature. When the NiTi embedded in the composites has negligible prestrain, as is the case with composites 1 and 3, the thermally induced strain is calculated by

$$\epsilon_{TE}(T) = \alpha_{comp}(T)\,\Delta T. \tag{6}$$

Table 2. Results from axial stiffness tests.

Sample	Temperature [°C]	Composite Modulus [GPa]	Relative Δk
Al Reference	23	75.46	-
	58	68.87	-8.7%
	98	67.51	-10.5%
Composite 1	23	56.83	-
	59	56.98	0.30%
	98	58.43	2.80%
Composite 2	24	56.24	-
	58	57.22	1.70%
	99	61.84	10.00%
Composite 3	23	42.24	-
	58	42.97	1.70%
	98	27.11	-35.80%

Unlike composites 1 and 3, composite 2 also has a recovery region that is taken into account. The difference in the strain due to CTE and the observed strain in composite 2 is due to the shape memory effect of the embedded NiTi. Since the composites are not mechanically loaded there is no other mechanism for creating a negative strain. The recovery strain, ϵ_{rec}, is quantified as the difference in strain induced through the composite thermal expansion alone, as calculated by (6), and the average of the heating and cooling strains while the composite is in the high temperature region. The recovery strain was found to be $-190\ \mu\epsilon$ and added to the thermal expansion strain to find the total thermal strain,

$$\epsilon\left(T\right) = \alpha_{comp}\left(T\right)\Delta T + \left(1-\zeta\right)\epsilon_{rec} \tag{7}$$

where α_{comp} is given by (3). Using this equation, the modeled thermal strain is compared with the observed strain in Fig 3.

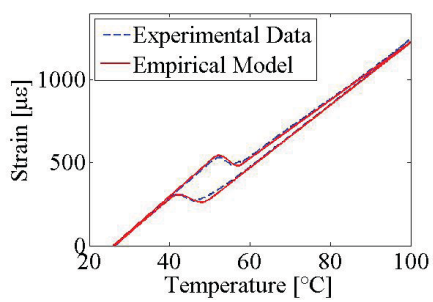

Figure 3. Thermally induced strain of composite 2 and empirical model.

2.2.2 Static axial stiffness tests

The results from the static axial stiffness tests are seen in Table 2. Since the cross sectional dimensions were varied to increase volume fraction, effective moduli values are presented to normalize the results with respect to geometry. Since modulus and axial stiffness are proportional and assuming constant composite length and cross sectional area during testing, relative change in modulus is equal to relative change in axial stiffness which is calculated by

$$\Delta k\left(T\right) = \Delta E\left(T\right) = \frac{E\left(T\right) - E_{RT}}{E_{RT}} \times 100\% \tag{8}$$

where E_{RT} is room temperature composite modulus and $E\left(T\right)$ is composite modulus at test temperature, T.

Table 3. Results from NiTi-Al composite axial natural frequency tests.

Composite	Temperature [°C]	Natural Frequency [Hz]	Relative $\Delta\omega_n$
Al Reference	24	1882	-
	102	1637	-13.0%
Composite 1	24	1972	-
	104	1715	-13.0%
Composite 2	24	1563	-
	102	1492	-4.5%
Composite 3	23	1492	-
	103	1492	0.0%

The Al reference sample continually decreases in stiffness as temperature increases. This is due to the elastic modulus of the Al decreasing with increasing temperature. Composites 1 and 2 both show increasing stiffness with increasing temperature. Further, composite 2 has a greater increase in stiffness than composite 1 at both elevated temperatures. The increase in modulus indicates that the embedded NiTi ribbons are transforming to austenite as temperature increases. The increasing elastic modulus of NiTi through the $M - A$ transformation is offsetting the decrease in modulus of the Al matrix and causing a net increase composite stiffness. As the NiTi content increases, the relative modulus change also increases.

Composite 3 shows an initial increase in stiffness at 58°C, consistent with composites 1 and 2, but then a significant decrease in stiffness at 98°C. The load-displacement data from the load frame for this test shows that at the nominal 100°C test temperature, composites 1 and 2 exhibit a nearly linear trend while composite 3 shows a trend consistent with a superelastic shape memory alloy, Fig. 4. Above 35 N, composite 3 exhibits a region with a much lower force-displacement slope, indicative of a stress induced $A - M$ transformation. This large increase in displacement associated with detwinning coupled with a transformation back to martensite would cause composite 3 to exhibit a decrease in stiffness at 100°C. Composites 1 and 2 may also exhibit such behavior at this temperature but will require a larger load to begin the $A - M$ transformation due to their smaller volume fractions on NiTi and larger cross sections, as the smaller volume of NiTi will carry a smaller fraction of the applied stress.

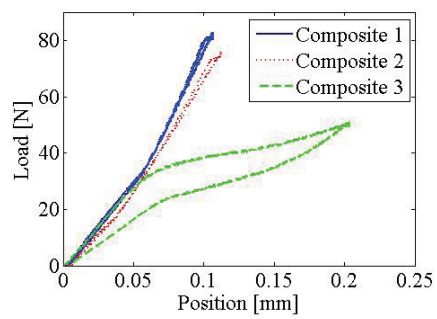

Figure 4. Load versus displacement plot for NiTi-Al composites 1, 2, and 3 at 100°C.

2.2.3 Axial natural frequency tests

Results from the axial natural frequency tests are shown in Table 3. The results show that the composites do not create an increase in natural frequency with increasing temperature but do exhibit a linear trend between $\Delta\omega_n$ and NiTi volume fraction. The relative decrease in natural frequency becomes smaller as the NiTi volume fraction increases. This trend continues with composite 3 having no change in natural frequency at 103°C with respect to its natural frequency at room temperature. This indicates that the NiTi is having an effect on the axial natural frequency at temperature via the $M - A$ transformation, offsetting the temperature induced reduction in modulus of the Al with the modulus increase of the NiTi.

The axial natural frequency of a rod or column is related to the axial stiffness through

$$\omega_n = \sqrt{\frac{k}{m}} \tag{9}$$

where m is the point mass of the dynamic system. Since composites 1 and 2 exhibit an increase in axial stiffness relative to room temperature at 100°C, a corresponding increase in ω_n is expected. From the Table 3 we see a decrease in natural frequency for these composites. Also, the axial stiffness of composite 3 in Table 2 suggests that it should have the lowest stiffness of all tested samples, however it experiences no change in ω_n. This is due to the loading of the composite. As the $A - M$ transformation is stress dependent, the force generated by the acceleration of the end mass is not enough to cause the NiTi ribbons in composite 3 to undergo the $A - M$ transformation observed in the stiffness tests. With no stress induced transformation, the NiTi ribbons remain austenitic and counteracts the decreasing stiffness of the Al matrix over a low loading range.

A hypothesis for the observed decrease and unchanged axial natural frequencies of the composites is that in heating the composites, thermal expansion of the Al matrix places a tensile load on the embedded NiTi. This tensile load increases with temperature and rather than having an unstrained transformation of the embedded NiTi, the ribbons undergo a partially constrained transformation, placing a compressive stress on the matrix. In observing the natural frequency of beams and rods, a compressive load will serve to reduce the natural frequency with respect to the unloaded structure. This compressive stress offsets any gains in natural frequency induced by the $M - A$ transformation. Ongoing work is focused on the development of analytical models to describe the effects of prestrain on the embedded NiTi, the resulting recovery stresses, and their effect on the dynamic behavior of the composites.

3. GALFENOL-ALUMINUM UAM COMPOSITES

3.1 FeGa-Al composite methods

3.1.1 Composite construction

An FeGa-Al composite was constructed using a FeGa piece 0.381 mm (0.015 in) thick and 10.0 mm (0.394 in) wide consisting of 18.4 at.% Ga and 1002 low carbon steel additions with magnetic domains oriented in the $\langle 100 \rangle$ direction, along the length of the strip. The FeGa strip was placed in a groove machined in Al 3003-H18 plate to remain flush with the welding surface and was secured to the bottom of the plate using strain gauge adhesive. After embedding, the composite was machined to a width of 25.4 mm (1 in) and a thickness of 1.27 mm (0.050 in). After machining, the composite had a small section of exposed FeGa, as shown in Fig. 5, to be used as reference material in testing. In order to amplify motion in actuation testing and increase response to bending in sensing applications, the composite was designed with the FeGa strip placed 0.102 mm (0.004 in) above the midplane of the composite to ensure that any induced or generated stress is completely tensile or compressive.

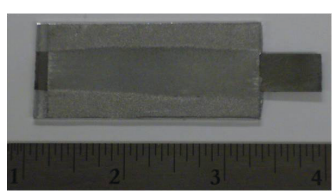

Figure 5. Machined FeGa-Al UAM composite 3.

3.1.2 Actuation tests

Strain gages were applied to the FeGa-Al composite on the exposed FeGa and on the top and bottom surfaces of the composite directly above and below the embedded FeGa. These gages were used to measure the strain generated along the direction of the FeGa strip. The composite was suspended in an electromagnetic drive coil while flux was measured at the tip of the exposed FeGa using a Hall probe. The drive coil was used to create an alternating magnetic field to saturate the FeGa while signals from the strain gages were recorded.

3.2 FeGa-Al composite experimental results and discussion

The FeGa-Al composite exhibits a strain response to the applied magnetic field as shown in Fig. 6. The strain responses of both the exposed FeGa and top surface of the composite show flat regions indicative of magnetic saturation. The strain at the bottom of the composite also reaches a minimum when the FeGa strip becomes saturated. The exposed FeGa exhibits a maximum strain of 193.5 $\mu\epsilon$, which is typical for this alloy.[16] The composite exhibits a 52.4 $\mu\epsilon$ response on the top surface and a -4.92 $\mu\epsilon$ response on the bottom surface.

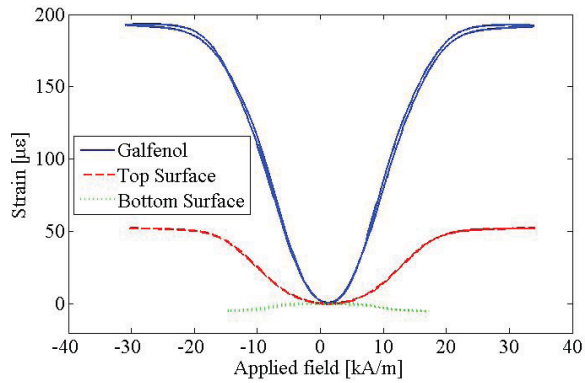

Figure 6. FeGa-Al composite strain versus magnetic field plot.

The difference in strain as measured on the exposed FeGa and measured on the composite surface could be due to two causes. First, there could be imperfect coupling between the FeGa strip and Al matrix. This would result in the FeGa strip applying load through only a portion of its magnetostrictive cycle as it would move relative to the matrix during other portions. The second scenario assumes perfect coupling and the lower composite strain is due to a loading effect on the FeGa strip from the surrounding Al matrix; the FeGa strip has a reduction in total strain due to the elastic response of the Al matrix as the active material causes composite deformation.

To investigate the nature of the coupling between the matrix and embedded FeGa, a series of simple calculations were made based upon the maximum theoretical stress FeGa can apply. This calculation assumes perfect coupling through strain continuity as a function of height and complete transfer of the load generated by the FeGa strip to the Al matrix. Using the known location of the FeGa strip within the composite, the elastic modulus of the Al matrix (68 GPa[17]), and a modulus of 57 GPa for the magnetically saturated FeGa,[18] the neutral bending axis of the composite was calculated and found to be at 0.6299 mm (0.0248 in) from the bottom surface of the composite, nearly coinciding with the composite midplane. This results in the FeGa midplane being 0.2972 mm (0.0117 in) above the neutral axis thus applying an axial load and bending moment during the actuation tests.

Next, actuation of the composite was treated as a force being applied over the FeGa strip cross section. The force was calculated by multiplying the magnetostriction at saturation of the FeGa element, ϵ_{sat}, by its elastic modulus, then dividing the resulting stress by the cross sectional area of the FeGa. The estimated force is given by

$$F = \frac{E\epsilon_{sat}}{tw} \tag{10}$$

where t and w are the thickness and width of the FeGa element, respectively. The axial and bending stresses are calculated by

$$\sigma_a = \frac{F}{tw} \tag{11}$$

and

$$\sigma_b(z) = \frac{F(0.2972)z}{I_{comp}}, \tag{12}$$

respectively, where z is the height at which the stresses are calculated, and I_{comp} is the moment of inertia for the entire composite. Using the total calculated stresses, the strain as a function of composite height is calculated by

$$\epsilon(z) = \frac{\sigma_a + \sigma_b(z)}{E_{comp}}, \tag{13}$$

where E_{comp} is the composite modulus as calculated through a rule of mixtures.

Using this calculation, the strains in the composite at the top and bottom fiber are found to be 45.50 $\mu\epsilon$ and -7.42 $\mu\epsilon$, respectively, when the FeGa element is saturated. These strain values are similar to what is observed from the experiment. The differences between the observed and calculated strains come from assuming full transformation of the free magnetostriction of the FeGa element to blocking stress and assuming the rolled FeGa material used in the composite has mechanical properties equal to those found in literature. However, the preliminary strain estimates from the simple model suggest that there is strong mechanical coupling between the FeGa strip and the Al matrix which is critical for magnetic sensing and actuation. Ongoing work is focused on characterization of the rolled FeGa material and development of FEA models of the rolled FeGa material as well as the sensing and actuation properties of the composite. The models in development will also be useful in designing the next generation of FeGa-Al composites.

4. POLYVINYLIDENE FLUORIDE-ALUMINUM UAM COMPOSITES

4.1 PVDF-Al composite methods

4.1.1 Composite construction

A PVDF-Al composite was created by embedding a thin electroactive PVDF film to achieve embedded force sensing. Prior to embedding, a 140 mm (5.5 in) long, 3.175 mm (0.125 in) wide piece of PVDF with deposited electrodes was encased in polyimide tape. The resulting sensor was attached to an amplifying circuit to observe its response to external pressure excitation prior to embedding. The sensor exhibited a capacitance of approximately 2 nF and no electrical continuity between the electrodes. The sensor was next embedded by placing it in a 0.152 mm (0.006 in) deep channel in an Al 3003-H18 baseplate and welding over top of the channel.

Also constructed, for the purpose of comparison, was a 19 mm by 40 mm (0.75 in by 1.6 in) rectangular PVDF sample insulated with polyimide film on both sides. This replicates the PVDF element embedded within the Al matrix for the purpose of characterizing the film without the effects of the surrounding Al matrix.

4.1.2 Harmonic load tests

The reference PVDF and PVDF-Al composite were given a harmonic load using a magnetic actuator with a load cell installed in series. The actuator contacted the PVDF samples through a 3.175 mm (0.125 in) diameter circular loading face. PVDF signals were monitored through a voltage amplifying circuit with a high pass cut-off frequency of 5.9 Hz while a 60 Hz notch filter was used to reduce electrical noise. The experimental setup is shown in Fig. 7.

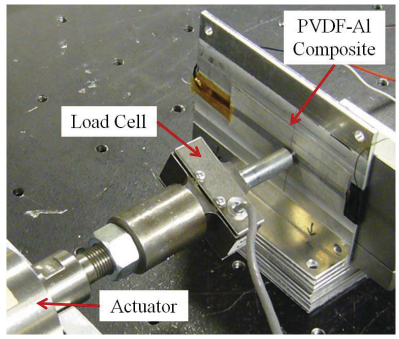

Figure 7. PVDF-Al composite sensing test setup.

Initial tests gave a mechanical excitation to both samples at 212 Hz. This frequency was chosen in order to avoid 60 Hz noise and its harmonics. The samples were next excited through a stepped sine test with a frequency range of 10 Hz to 1000 Hz and initially preloaded so there was persistent compressive load on the sensors. The compressive bias was used to maintain contact between the load face and samples, thus preventing impact loading. The signal from the persistent preload is filtered out by the high pass filters in the conditioning circuit.

4.2 PVDF-Al composite experimental results and discussion

In initial testing at a discrete frequency, the frequency spectra from both the reference PVDF and PVDF-Al composite, Fig. 8 (a), show strong signal peaks at 212 Hz, the frequency of mechanical excitation. This shows that the PVDF element remains active and undamaged from the embedding process. Though peaks corresponding to the excitation frequency are prominent in the PVDF-Al composite signal, they are of similar magnitude to the signal from 60 Hz noise and its harmonics.

The transfer function of signal response to load input for the reference PVDF and embedded composite can be seen in Fig. 8 (b). The response of the reference sample has a peak at 630 Hz while the PVDF-Al composite has a peak in magnitude at 710 Hz. The shift in peak magnitude is likely a result of dynamics in the surrounding Al matrix in the PVDF-Al composite.

While the trends observed in the frequency responses are similar, the magnitude of the embedded sample is significantly lower in magnitude than the reference PVDF. This reduction in magnitude is expected because instead of directly supporting any applied load, as in the case of the reference PVDF, the embedded PVDF supports a smaller amount of load due to support from the Al layer above and surrounding Al matrix. A simple way of overcoming this is by increasing gain in the conditioning circuit.

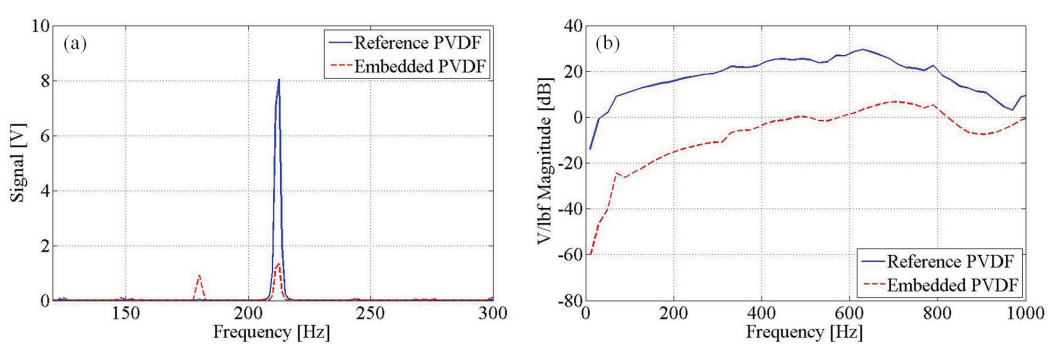

Figure 8. Results from PVDF reference and PVDF-Al composite tests: (a) discrete frequency test (b) signal/load magnitude frequency response.

Future PVDF-Al characterization tests will apply non-harmonic inputs such as impact or step loading. In addition to these tests, the sensitivity of the composite to off-center loading, loads applied at a distance from the

embedded PVDF element, will be conducted. This will allow for the use of multiple embedded PVDF elements to detect not only the magnitude of an applied force, but its location on the composite surface.

5. SUMMARY

In this research we have studied active composites made from NiTi, FeGa, and PVDF embedded in an Al matrix. For NiTi-Al composites we have observed their unique behavior and identified the underlying phenomena that govern thermally induced strain, thermally variable stiffness, and dynamic properties. An empirical model has been developed to describe the thermally induced strain behavior. We have also observed up to a 10.0% increase in axial stiffness relative to room temperature when heating the composites to 100°C and a reduction in the decrease in natural frequency through the $M - A$ transformation. Future work with NiTi-Al composites includes rigorous analytical modeling on NiTi-Al composites to describe their thermomechanical behavior including the effects of NiTi prestrain and recovery stresses.

We also investigated the coupling between magnetostrictive FeGa and the Al matrix through actuation testing. Simple calculations indicate that the magnetically induced strain in the FeGa phase is transfered to the magnetically inert Al matrix indicating good coupling between the composite constituents. This coupling is vital for the next series of tests which will measure the magnetic response of the embedded FeGa to stresses applied to the composite.

We have performed harmonic testing on a PVDF-Al composite and quantified its electrical response. The tests have quantified the frequency response of embedded PVDF to an applied load. Future testing will include non-harmonic loads such as impulses and step loads in addition to the composite response to distant loads which will enable composites to detect impact location as well as magnitude.

ACKNOWLEDGMENTS

The authors would like to acknowledge Matt Short, Matt Bloss, and Karl Graff from the Edison Welding Institute for their assistance and use of UAM equipment. The NiTi ribbon was provided by Nitinol Devices and Components. Financial support for this research was provided by the member organizations of the Smart Vehicle Concepts Center (www.SmartVehicleCenter.org), National Science Foundation Industry/University Cooperative Research Center Program (I/UCRC), and Smart Vehicle Concepts Graduate Fellowship Program.

REFERENCES

[1] Chawla, N., "Metal matrix composites in automotive applications," Advanced Materials and Processes, 164, 29–31 (2006).

[2] Graff, K., [New Developments in Advanced Welding], Woodhead Publishing Limited, Cambridge, 241 (2005).

[3] DeVries, E., "Mechanics and mechanisms of ultrasonic metal welding," PhD Thesis, The Ohio State University, Columbus, OH (2004).

[4] Hartl, D. and Lagoudas, D., [Shape Memory Alloys], Science and Business Media, LLC, New York, Chapter 2 (2008).

[5] Johnson Matthey, "Surface strains in Nitinol wire, ribbon and sheet, " jmmedical.com (2011).

[6] Gori, F., Carnevale, D., Atan, A. D., Nicosia, S., and Pennestri, E. , "A new hysteretic behavior in the electrical resistivity of Flexinol memory alloys versus temperature, " International Journal of Thermophysics, 27 (3), 866–879 (2006).

[7] Uchil, J., Mahesh, K. K., and Kumara, K. G., "Electrical resistivity and strain recovery studies on the effect of thermal cycling under constant stress on R-phase in NiTi shape memory alloys," Physica B, 324, 419–228 (2002).

[8] Scalea, F. L., "Measurement of thermal expansion coefficients of composites using strain gauges," Experimental Mechanics, 328, 233–241 (1998).

[9] Kaufman, J., "Aluminum alloy database," knovel.com (2004).

[10] Vokoun, D., Kafka, V., and Hu, C. T., "Recovery stresses generated by NiTi shape memory wires under different constrain conditions," Smart Materials and Structures, 12, 680–685 (2003).

[11] Clyne, T. and Withers, P., [An Introduction to Metal Matrix Composites], Cambridge University Press, Cambridge, 12–14 (1993).

[12] Staab, G., [Laminar Composites], Butterworth-Heinemann, Boston, 92 (1999).

[13] Sittner, P., Michaud, V., and Schrooten, J., "Modeling and material design of SMA polymer composites," Materials Transactions, 43 (5), 984–993 (2002).

[14] Sittner, P., and Stalmans, R., "Developing hybrid polymer composites with embedded shape-memory alloy wires," JOM, 52 (10), 15–20 (2000).

[15] Brinson, L., "One dimensional constitutive behavior of shape memory alloys," Journal of Intelligent Material Systems & Structures, 4 (2), 229–242 (1993).

[16] Mahadevan, A., "Force and torque sensing with Galfenol alloys," MS Thesis, The Ohio State University, Columbus, OH (2009).

[17] Kaufman, J., ed., [Properties of Aluminum Alloys: Tensile, Creep, and Fatigue Data], The Aluminum Association, Inc. and ASM International, Materials Park (1999).

[18] Kellogg, R. A., Flatau, A., Clark, A. E., Wun-Fogle, M., Lograsso, T., "Quasi-static transduction characterization of Galfenol," Journal of Intelligent Material Systems and Structures, 16, 471–479 (2005).